



Comparative study of soft computing models for prediction of scour below two symmetric crossing jets

Shayan Naini¹ · Hojat Karami² · Khosrow Hosseini²

Received: 5 May 2022 / Accepted: 7 October 2022 / Published online: 1 November 2022
© Saudi Society for Geosciences 2022

Abstract

The scour estimation downstream of the dam's hydraulic structures is a serious issue and has long been considered an important topic by hydraulic engineers. The literature shows that the computational methods are good alternatives for predicting the scour in hydraulic structures in which the conventional methods demonstrate shortcomings. In the present paper, various machine learning techniques have been used for the first time to predict the scour below the two symmetric crossing jets. Four types of artificial neural networks (ANNs), including feedforward back-propagation (FFBP), cascade-forward back-propagation (CFBP), radial basis function (RBF), generalized regression neural network (GRNN) along with the adaptive neuro-fuzzy inference system (ANFIS), and support vector regression (SVR) were employed and evaluated. Two important scour hole characteristics, namely the maximum scour hole depth and its location relative to the scour hole origin, were predicted at three crossing angles. The soft computing models were also compared with the traditional empirical methods. The results indicated that the applied computing techniques perform satisfactorily and improve the results remarkably. They can estimate the scour more precisely than the regression models and can be considered robust alternative tools. A detailed sensitivity analysis was also performed on the FFBP that shows the crossing angle has a powerful effect on the predictions. The SVR improved the results to 47% and 31.71% for the scour hole depth and its location, respectively, in terms of the correlation coefficient.

Keywords Machine learning methods · Regression equations · Scour below crossing jets

Introduction

The scour downstream of hydraulic structures such as the spillways and orifices can be catastrophic, endangering the dam's stability and the side structures. This phenomenon has been an important research subject in hydraulic engineering. Most of the research performed in the past is on the single jet scour (Rajaratnam and Mazurek 2002; Pagliara et al. 2008; Kartal and Emiroglu 2022; Palermo et al. 2021; Chen et al. 2022; Sá Machado et al. 2019; Bombardelli et al. 2018), who

studied the scour and presented formulae for estimating the scour hole depth and dimensions.

Few studies have been carried out on the crossing jets scour. The crossing jets are formed when the middle orifices of a dam or their outlet systems are open. The crossing jets are designed in the dams as a solution for dissipating the energy of the erosive jet; this process is accomplished through colliding the jets in the air. However, the scour at the plunge pools can still occur.

Pagliara et al. (2011) conducted an experimental study on the scour caused by two symmetric crossing jets. They presented specific equations for estimating the scour hole dimensions below the crossing jets. Due to the complexity of the phenomenon, their formulae were proposed separately at three different crossing angles of $\alpha_c=30^\circ$, 75° , and 120° . Pagliara and Palermo (2013) studied the scour caused by the collision of two symmetrical jets in aerated mode, and it was concluded that the air profoundly changes the scour morphology. Pagliara and Palermo (2017) analyzed the impact of vertical non-colliding jets at multiple angles

Responsible Editor: Broder J. Merkel

✉ Hojat Karami
hkarami@semnan.ac.ir

¹ Department of Water Engineering and Hydraulic Structures, Faculty of Civil Engineering, Semnan University, Semnan, Iran

² Faculty of Civil Engineering, Semnan University, Semnan, Iran

where the virtual colliding point was considered beneath the bed. They provided relationships to predict the main parameters of the scour, including the maximum scour depth. Naini et al. (2022) conducted laboratory research on the scour due to the symmetric crossing jets with a bed material of $d_{50}=1.4\text{mm}$. Because of the high complexity of the phenomenon, the proposed equations, which included the crossing angle as an independent variable, failed to predict the scour hole parameters accurately at arbitrary crossing angles. However, the formulae presented for each separate angle yielded satisfactory results. The other researchers in the literature who worked on multiple jets can be mentioned as Latifi et al. (2018), Uyumaz (1988), and Mehraein et al. (2012), which all denoted that using multiple jets reduces the scour compared with the single jet.

In the case of the crossing jets, estimating the scour could be more difficult due to the interaction of the flow with air and sediments, which makes it a highly complex phenomenon. Therefore, the conventional approaches like the traditional regression could not estimate the scour characteristics accurately owing to the associated limitations.

The application of machine learning methods such as the adaptive neuro-fuzzy inference system, ANNs, and support vector regression has been confirmed to be beneficial in hydraulic and water resources engineering problems such as erosion and scour prediction, mainly due to their learning capabilities.

Examples of artificial intelligence (AI) methods for estimating the scour can be seen in the literature. Azmathullah et al. (2005) and Naini (2011) employed the ANNs for estimating the scour hole dimensions below ski-jump spillways. They concluded that the ANNs are superior to the traditional regression equations. Mohammadpour (2017) estimated the local scour around piers using M5-Tree, gene expression programming (GEP), and ANNs; he concluded that the radial basis function (RBF) network yields better results than the other methods, including conventional equations.

Riahi-Madvar et al. (2019) applied five models, including the ANFIS, RBF, multilayer perceptron (MLP), and regression for predicting the scour geometry of grade-control structure; they observed that ANFIS and MLP present higher accuracy. Seyedian et al. (2022) developed soft computing models such as extreme learning machine (ELM), GEP, and SVM for the scour depth of grade-control structures; it was confirmed that GEP is more robust than the other methods.

Bonakdari et al. (2020) predicted the abutment scour depth using ELM. They used eleven input combinations to investigate the effect of each parameter on the scour depth. It was observed that a four-input combination yields a better accuracy, and the ELM outperforms the regression equations. Azimi et al. (2019) applied ANFIS with singular value decomposition (SVD) and genetic algorithm (GA) to predict the abutment scour depth; it was revealed that

the ANFIS-GA/SVD has higher accuracy than the other approaches.

Shahbazbeygi et al. (2021) simulated the scour around cross-vane structure with generalized structures group method of data handling (GSGMDH); it was found that the GSGMDH scheme is more flexible and superior to the group method of data handling.

Adib et al. (2020) applied ANNs, ANFIS, SVM, and GA to predict the scour depth in group piers; it was revealed that the MLP-GA and RBF-GA are the best models in terms of the error criteria. Ebtehaj et al. (2018) employed ELM, SVM, and ANN techniques to predict the scour depth at pile groups; they reported on the superiority of the ELM over the other methods. The most effective parameter on scour was found using multiple input combinations. Also, an equation based on the ELM was proposed for practical uses.

Parsaie et al. (2019) used the SVM, ANN, and ANFIS for estimating the scour of a pipeline in the river, and the SVM results were more accurate. Hassanzadeh et al. (2019) used an optimized ANFIS with multiple optimization methods to estimate the scour depth in the bridge pier; the results showed that the new methods are highly efficient in the predictions. Kaveh et al. (2021) presented a hybrid method combining the grasshopper optimization algorithm with the feedforward neural network for predicting the scour depth pattern around bridge piers; the results indicated that the proposed model has higher accuracy and improved the results. Sharafati et al. (2020a) predicted the scour depth downstream of weirs by integrating the ANFIS with various optimization algorithms; the results indicated that hybridizing the ANFIS with invasive weed optimization offers the highest accuracy. Rashki Ghaleh Nou et al. (2019) simulated the scour depth around the submerged weirs using the self-adaptive extreme learning machine (SAELM); the results were compared with the ANN and SVM; SAELM outperformed the other models. Sammen et al. (2020) predicted the scour depth below the ski-jump spillway by combining the ANN with three optimization algorithms; the results showed that the ANN hybridized with the Harris Hawks optimization is more efficient than the other methods. Sun et al. (2021) used a hybrid method combining the fruit fly optimization algorithm (FOA) with the SVR for estimating the scour features below ski-jump spillways. The results indicated that the FOA-SVR method remarkably improved the results and outperformed the regression models.

Other recent studies that contribute to the AI technique application in the hydraulic and water resources fields can be mentioned briefly (Band et al. 2021; Yaseen et al. 2019; Hu et al. 2021; Hoang et al. 2018; Samet et al. 2019; Sharafati et al. 2021; Hassanvand et al. 2018; Das et al. 2019; Yaseen 2020; Malik et al. 2020; Salih et al. 2019; Sharafati et al. 2020b; Campos and Pedrollo 2021; Nivesh et al. 2022; Tao et al. 2021).

To the authors' knowledge and by surveying the literature, predicting the scour features below the symmetric crossing jets with AI approaches has not been investigated yet. Therefore, the main objective of this research is to apply and evaluate the various soft computing models as an alternative approach to predict the principal features of the scour below the symmetric crossing jets, i.e., the maximum scour hole depth and its location relative to the origin. Four types of neural network schemes (FFBP, CFBP, RBF, and GRNN), with the ANFIS and SVR, were utilized. Before the modeling and comparative analysis of the various methods, a detailed sensitivity analysis was accomplished with the feedforward back-propagation (FFBP) network to assess the impact of each parameter and to find the most effective input combination. The non-dimensional and dimensional combinations of inputs were employed to identify the superior FFBP models. Then, the best non-dimensional input combination was chosen for the modeling in the other techniques.

The performance of the computing methods is evaluated on the training and testing datasets. One of the essential aims of this research is to develop superior computational models capable of estimating and interpolating the scour hole features at various arbitrary crossing angles between $30^\circ < \alpha < 110^\circ$. This strategy has not been considered in the previous research by the regression models, mainly due to the high complexity of the scour phenomenon and regression method limitations. A comparison is made with the regression formulae obtained from the current research dataset and previous research to evaluate the developed models.

The current study shows that by considering the crossing angle as an independent parameter in the nonlinear regression equations, the regression models fail to estimate the maximum scour hole depth and its location precisely, unlike the AI techniques.

The efficiency of the methods is assessed by the quantitative error criteria and graphical diagrams. For providing the required data, an experimental work was conducted, and data series were gathered.

Material and methods

Artificial neural networks

ANN was presented by McCulloch and Pitts (1943) as a mathematical concept. A neural network is made of nodes called neurons which are simple processing units. An artificial neural network is a mathematical model consisting of neurons distributed in one or more layers. The most common ANN has three layers: the input layer where data are fed, a hidden layer consisting of neurons that receive the outputs from the previous layer and produce their outputs to be entered into the next layer, and the output layer that makes

the favorite output. Among the multiple kinds of ANNs, four networks, i.e., the FFBP, CFBP, RBF, and GRNN, were utilized in the current research that are briefly described below.

Feedforward back-propagation

A common FFBP has an input, a hidden, and an output layer. The weighted inputs from the input layer are received and processed by the hidden layer through activation functions of neurons. Then the outputs enter the neurons in the next layer (output layer). The layers that contain the activation functions are the hidden and output layers, respectively. Figure 1 shows a typical FFBP network with three inputs and two outputs.

The networks can be trained or calibrated using data, and this process modifies the weights between the consecutive layers, which connect the neurons in multiple layers. The calibration continues until the output error between the estimated and experimental values becomes low and logical during the training.

The ANN models were developed via writing codes in MATLAB[®]. For training the FFBP and regulating the weights, the Bayesian regularization based on Levenberg-Marquardt optimization was adopted with the back-propagation procedure. This algorithm produces more generalization in the results (MacKay 1992). For obtaining the best FFBP networks, several attempts were made through trial and error, where the error between the experimental and estimated scour values becomes minimum. Namely, neurons in the hidden layer were added gradually, and the response was measured in the output. Also, different transfer functions such as the Tan-sigmoid and Log-sigmoid were examined for this goal. Finally, the optimal networks were selected for the assessments. For more information, readers can refer to Haykin (1994) and the MATLAB[®] user guide.

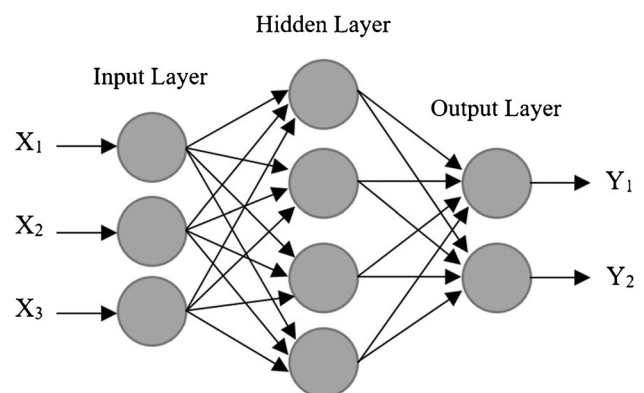


Fig. 1 FFBP structure

Cascade-forward back-propagation

In the cascade-forward back-propagation scheme, the hidden and output layers get inputs from their previous layers, including the input layer. Like feedforward nets, a cascade-forward network can learn any input-output relationship. For training the CFBP, the back-propagation learning method with Bayesian regularization was employed.

Radial basis function

The RBF fits a radial basis function neural network, which is a feedforward, supervised learning network with an input layer, a hidden layer called the radial basis function layer, and a linear output layer. The unique property of the RBF is its hidden layer. The inputs of the neurons in this layer are different than the FFBP. The radial basis function's input is the difference between weights and inputs multiplied by the bias. There are no weights between the input and hidden layers. The most conventional radial basis function is a Gaussian function as follows:

$$\varphi_i(r) = \exp \left[-\frac{\|x - w_i\|^2}{2\sigma^2} \right] \tag{1}$$

$\varphi_i(r)$ is the activation level of each hidden RBF neuron. In a radial basis function, $(x - w_i)$ is the distance from the center of the cluster. σ is the width of the function. The weights (w_i) represent the center of the clusters. If a hidden neuron receives an input pattern, the distance is calculated. An input with zero value would produce an output equal to 1; i.e., by reducing the distance between the x and w_i , the output is increased.

The output of the RBF is estimated as the weighted sum of the output value:

$$d(x) = \sum_{i=1}^H c_i \varphi_i(r) \tag{2}$$

In which c_i is the output for each hidden neuron. The training of an RBF is performed in two stages. At first, the centers of the units (w_i) are determined, which is a necessary process. This could be achieved with the k-means clustering approach. Then, the second task is determining the weights between the hidden (RBF) and output layers. In MATLAB, the spread constant value in the radial layer was changed for the training process in a trial and error approach to find the optimum model. For the current study, the RBF model receiving five inputs and producing two outputs (y_m/D_{eq} , l_m/D_{eq}) was developed.

One benefit of the RBF over the FFBP is that it is less time-consuming than the back-propagation networks. For

more information, refer to Haykin (1994) and Jang et al. (1997).

Generalized regression neural network

The GRNN was first introduced by Specht (1991). A GRNN has an architecture similar to the RBF and has a radial basis hidden layer and a particular output linear layer. The GRNN is slightly different than the RBF in the output layer. A GRNN comprises four layers, the input layer, pattern layer, summation layer, and output layer. Figure 2 shows a typical GRNN with three inputs.

The input layer is defined according to the number of inputs. The first layer is connected to the next layer (pattern layer). The pattern layer neurons consist of the tuneable RBFs. The neurons of this layer process the samples, which, the normal distribution is at the center of each training data. The next layer is the summation layer. There are two types of neurons in the summation layer, S and D . The S unit estimates the sum of weighted signals coming from the pattern neurons; they are weighted with the corresponding output of the training data (y_i). The signals going into the D unit of the summation are not weighted. The output is computed in the output layer as the S unit output divided by the D unit output as follows:

$$Y(x) = \frac{\sum_{i=1}^n y_i \exp(-d_i^2/2\sigma^2)}{\sum_{i=1}^n \exp(-d_i^2/2\sigma^2)} \tag{3}$$

d_i is the distance between the training sample and the predicted point. Similar to the RBF, for finding the favorite models, the spread value is changed in the training phase of the GRNN. A GRNN scheme with five inputs and two outputs (y_m/D_{eq} , l_m/D_{eq}) was built. Further details on the GRNN can be found in Specht (1991).

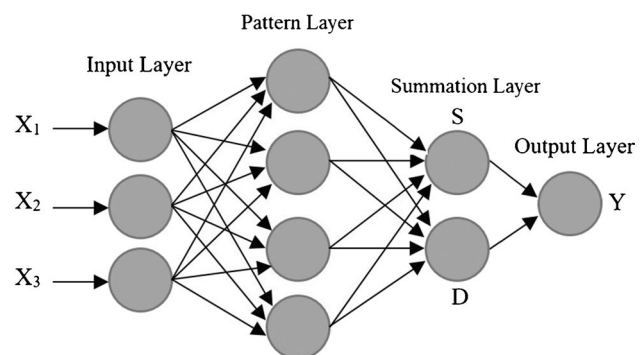


Fig. 2 GRNN structure

Adaptive neuro-fuzzy inference system

The ANFIS is a developed technique presented by Jang (1993) that can be used for modeling complicated phenomena. The ANFIS as a hybrid model integrates a fuzzy system with back-propagation training capability of a neural network that can update the parameters of membership functions in a Sugeno type fuzzy inference system utilizing the training dataset. The ANFIS uses fuzzy If-Then rules for the simulation. The hybrid training algorithm that is a combination of the back-propagation gradient descent and least-squares methods is used. As can be seen from Fig. 3, ANFIS is a five-layered scheme with a Sugeno inference system. The steps below show how the ANFIS functions with two fuzzy If-Then rules (Jang et al. 1997):

If x is A_1 and y is B_1 , then

$$f_1 = p_1x + q_1y + r_1 \tag{4}$$

If x is A_2 and y is B_2 , then

$$f_2 = p_2x + q_2y + r_2 \tag{5}$$

In which $p_i, q_i,$ and r_i are adjustable parameters. The membership functions are represented as A_1, A_2 and B_1, B_2 . x and y are the inputs. $O_{l,i}$ is the output of each node in every layer.

Layer 1: a function in this layer’s nodes determines the membership grade and can be demonstrated as below:

$$O_{1,i} = \mu_{A_i}(x) = \frac{1}{1 + |x - c_i/a_i|^{2b_i}} \tag{6}$$

In which $\mu_{A_i}(x)$ is a bell function; $a_i, b_i,$ and c_i are changeable parameters.

Layer 2: each node generates the output by multiplying the incoming inputs:

$$O_{2,i} = w_i = \mu_{A_i}(x)\mu_{B_i}(y) \tag{7}$$

Layer 3: the nodes are constant, and each node produces the normalized outcome as below:

$$O_{3,i} = \bar{w}_i = \frac{w_i}{w_1 + w_2} \tag{8}$$

Layer 4: every node output is estimated using the formula mentioned below:

$$O_{4,i} = \bar{w}_i f_i = \bar{w}_i(p_i x + q_i y + r_i) \tag{9}$$

Layer 5: a single node that computes the final output as below:

$$O_{5,i} = \sum_i \bar{w}_i f_i = \frac{\sum_i w_i f_i}{\sum_i w_i} \tag{10}$$

The Fuzzy Inference System was developed by subtractive clustering technique because the rules produced with this technique are minimized and developing the models with this method is fast. In this technique, the range of influence has to be determined.

The non-dimensional parameters were employed to predict the scour hole features. The MATLAB was used for the modeling, and two ANFIS models were developed for the maximum scour depth and its location. ANFIS structures with Gaussian membership functions were produced in a trial and error method. Hence, multiple values for the range of influence were determined to reach the highest accuracy in the training and testing data sets. Details of this technique can be found in Jang (1993).

Fig. 3 ANFIS structure

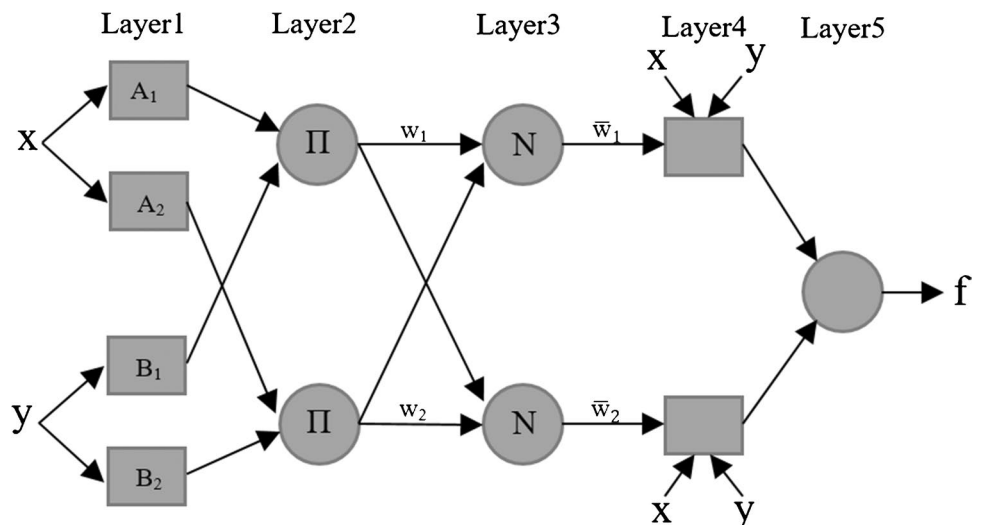


Table 1 Ranges of experimental raw data used

Variable	Q (m ³ /s)	h_0 (m)	S (m)	α_c (rad)	d_{90} (m)	y_m (m)	l_m (m)
Minimum	0.0013	0.03	0.05	0.524	0.0021	0.029	0.12
Maximum	0.00175	0.09	0.1	1.920	0.00315	0.142	0.35
Average	0.00152	0.060345	0.075287	1.221	0.002631	0.0973	0.21671
Standard deviation	0.00019	0.02449	0.02500	0.57002	0.000525	0.02526	0.04833

Support vector regression

The support vector machine is categorized as a data processing method. The SVM is used for classification and regression. When it is used for regression, it is usually called SVR. Nonlinear and complex problems can be modeled by this method with a suitable kernel function. And it has been widely utilized in the fields of hydraulic and water resources engineering.

It deals with minimizing the structural risk, which acts better than the neural network risk minimization.

The goal is detecting a function with a maximum ε deviation from the experimental targets. The function $f(x)$ is as follows (Smola and Scholkopf 2004):

$$f(x) = (\omega, x) + b, \quad \omega \in X, \quad b \in \mathbb{R} \quad (11)$$

In which ω is the weight and b is a coefficient, both calculated from the data. (ω, x) is the dot point in X . The value of ω has to be minimized in terms of the norm ($\|\omega\|^2 = (\omega, x)$) to ensure the flatness of the function (Vapnik 1995), which is an optimization process as below:

$$\text{minimize } \frac{1}{2} \|\omega\|^2 \quad \text{Subject to } \begin{cases} y_i - (\omega, x_i) - b \leq \varepsilon \\ (\omega, x_i) + b - y_i \leq \varepsilon \end{cases} \quad (12)$$

For modeling the SVM, the kernel type, such as the radial basis function, polynomial, multilayer perceptron, etc., and the regularization parameter (C), must be defined. Two SVR models were trained and built for the maximum scour depth and its location. This study used the RBF and polynomial as the proper kernels for the two SVR models producing the lowest output errors. In the present study, the simplex optimization algorithm was utilized to gain the optimum hyper-parameters of each kernel-based function. Accordingly, the RBF parameters were defined by γ and σ ; the polynomial parameters were defined by γ , r , and the polynomial degree. For details on the SVM, refer to Vapnik (1995) and Smola and Scholkopf (2004).

Experimental setup and dimensional analysis

For building and validating the soft computing models, experimental data were used. The experiments were carried out at the hydraulic laboratory of Semnan University

in a 16-m-long, 1-m-wide, and 0.8-m-deep rectangular channel. The crossing angle of the jets was considered three values of $\alpha_c = 30^\circ$, 70° , and 110° , and the vertical angle of the crossing jets was constant $\alpha_v = 45^\circ$. A total of 108 experiments were carried out. Table 1 shows the range and statistics of the parameters.

A gate at the end of the canal was used to adjust the tailwater level. A metal base was built to hold the jet pipes during the experiments. The colliding angle of the jets could be changed by the holder clamps. An electro pump with a maximum discharge of 0.01 m³/s and two circular pipes with an inner diameter of $D = 0.022$ m were used. The diameter of the equivalent single jet (D_{eq}) was chosen according to the criterion defined by Pagliara et al. (2011), having a cross-sectional area equal to the total cross-sections of the two crossing jets pipes calculated as $D_{eq} = \sqrt{2D^2}$ and was obtained equivalent to $D_{eq} = 0.0311$ m. The water discharge in the two jet pipes was equally regulated. The flow discharge in the main pipe was measured by an electromagnetic flowmeter. Figure 4 shows a view of the colliding jets and the scour.

Several parameters are involved in creating the scour below the crossing jets; the relationship can be as follows:

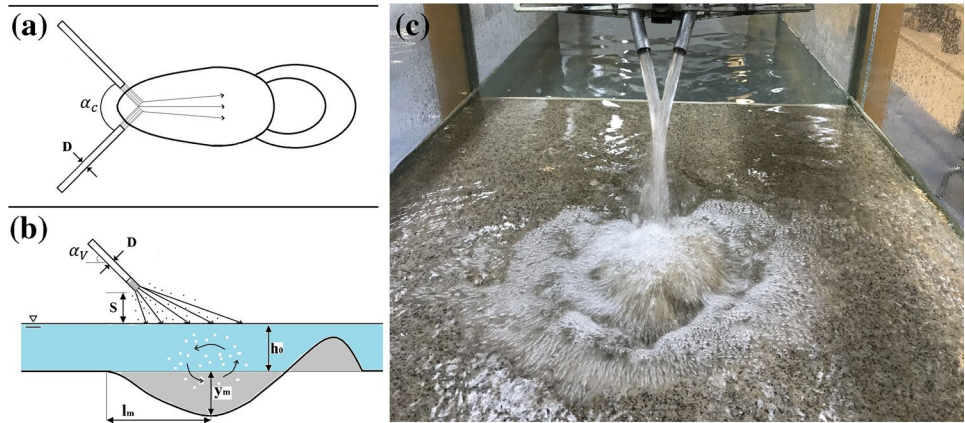
$$\phi = f(V, d_s, D_{eq}, \rho, \rho_s, \mu, g, S, h_0, \alpha_c) \quad (13)$$

where ϕ is one of the scour hole characteristics, such as the maximum scour hole depth (y_m) or the location of the maximum scour depth relative to the scour hole origin (l_m); V is the velocity of the water jets equal to $V = Q / (\pi D_{eq}^2 / 4)$; Q is the total discharge in the main pipe; D_{eq} is the equivalent single jet diameter; d_s is the particle size of the bed material; ρ is the water density; ρ_s is the sediment density; μ is the dynamic viscosity of water; g is the acceleration due to gravity; S is the vertical distance between the central point of the colliding jets and the water surface; h_0 is the tailwater depth; α_c is the angle of the crossing jets. By employing the Π theorem of Buckingham, the non-dimensional parameters are obtained as follows:

$$\left[\begin{array}{l} \pi_1 = \frac{\rho_s}{\rho}, \pi_2 = \frac{d_s}{D_{eq}}, \pi_3 = \frac{V^2}{gD_{eq}}, \pi_4 = \frac{\rho V D_{eq}}{\mu}, \\ \pi_5 = \frac{h_0}{D_{eq}}, \pi_6 = \frac{S}{D_{eq}}, \pi_7 = \frac{\phi}{D_{eq}}, \pi_8 = \alpha_c \end{array} \right] \quad (14)$$

Combining the dimensionless parameters of $\pi_1 = \rho_s / \rho$, $\pi_2 = d_s / D_{eq}$, and $\pi_3 = V^2 / gD_{eq}$, the dimensionless

Fig. 4 A schematic view of the **a** plan, **b** longitudinal section of the scour, and **c** colliding jets at $\alpha_c = 30^\circ$



parameter $V/\sqrt{gd_s((\rho_s - \rho)/\rho)}$ is obtained. Which is called densimetric Froude number and is shown as F_{d90} . According to the above explanations, the following equation can be presented:

$$\frac{\phi}{D_{eq}} = f \left[F_{d90}, \frac{h_0}{D_{eq}}, \frac{S}{D_{eq}}, \alpha_c, \frac{d_{90}}{D_{eq}} \right] \tag{15}$$

It should be noted that d_{90}/D_{eq} was solely considered an independent parameter in the analyses. The relationship (15) was employed for building dimensionless neural networks. Several long-term tests were carried out to determine the scour equilibrium stage and it was assessed that a 1-h test duration for each experiment would suffice.

The dataset was separated into two subsets; the training set, which contains 80% of the samples, was selected randomly for calibrating the AI techniques. The remaining 20% as the testing samples were considered to validate the models.

Nonlinear regression equations

According to the experimental data from the present study and Eq. (15) obtained from the previous section, the dimensionless nonlinear regression equations were derived based on the training dataset (80% data), which estimate the maximum depth of scour hole and its location relative to the origin. These equations are shown in Table 2. As can be seen from Table 2, α_c is included as an independent variable in Eqs. (16) and (17) to provide the estimations at the other arbitrary crossing angles between $\alpha_c = 30^\circ$ and 110° . The proposed equations from the previous study by Pagliara et al. (2011) were also utilized to evaluate and validate the current research models. These equations have been

presented for the scour hole depth at three different crossing angles separately, which can be seen in Table 2.

It should be noted that Pagliara et al. (2011) equations for $\alpha_c > 30^\circ$ pertain to the crossing angles of 75° and 120° , and due to a slight difference between them and those of the current study (70° and 110°), their results were compared with the developed schemes. The above relationships were validated by employing the same 20% data considered to be the testing data set.

Statistical measures

In the current work, four statistical measures were used to compare the results and evaluate the AI methods and the regression models. The Nash-Sutcliffe efficiency (NSE) varies between $-\infty$ and 1. If NSE approaches 1, the model is perfect. When NSE is negative, the observed mean value is a better prediction than the model. The correlation coefficient (CC), root mean square error (RMSE), and mean absolute error (MAE), which are defined by the following formulae:

$$CC = \frac{\left(\sum_{i=1}^n O_i P_i - \frac{1}{n} \sum_{i=1}^n O_i \sum_{i=1}^n P_i \right)}{\left(\sum_{i=1}^n O_i^2 - \frac{1}{n} \left(\sum_{i=1}^n O_i \right)^2 \right) \left(\sum_{i=1}^n P_i^2 - \frac{1}{n} \left(\sum_{i=1}^n P_i \right)^2 \right)} \tag{18}$$

$$NSE = 1 - \frac{\sum_{i=1}^N (O_i - P_i)^2}{\sum_{i=1}^N (O_i - \bar{O})^2} \tag{19}$$

$$RMSE = \sqrt{\frac{1}{n} \sum_{i=1}^n (O_i - P_i)^2} \tag{20}$$

Table 2 Empirical equations

Equation	α_c	No.
$\frac{y_m}{D_{eq}} = 2.088 (F_{d90})^{0.768} \left(\frac{h_0}{D_{eq}}\right)^{-0.195} \left(\frac{s}{D_{eq}}\right)^{-0.125} (\alpha_c)^{-0.146} \left(\frac{d_{90}}{D_{eq}}\right)^{0.456}$	$30^\circ \leq \alpha_c \leq 110$	(16)
$\frac{h_m}{D_{eq}} = 2.589 (F_{d90})^{0.792} \left(\frac{h_0}{D_{eq}}\right)^{-0.22} \left(\frac{s}{D_{eq}}\right)^{0.002} (\alpha_c)^{0.116} \left(\frac{d_{90}}{D_{eq}}\right)^{0.284}$	$30^\circ \leq \alpha_c \leq 110$	(17)
$\frac{z_m}{D_{eq}} = \left[\frac{0.3 F_{d90}}{\left(\frac{s}{D_{eq}}\right)^2} + \left(-0.046 \left(\frac{h_0}{D_{eq}}\right)^2 + 0.52 \frac{h_0}{D_{eq}} + 0.16\right) \right] \cdot \left[\left(0.003 \frac{h_0}{D_{eq}} - 0.02\right) \right]$	30°	Pagliara et al. (2011) (3a)
$\left(\frac{s}{D_{eq}}\right)^2 + \left(-0.05 \frac{h_0}{D_{eq}} + 0.24\right) \frac{s}{D_{eq}} + 1$		
$\frac{z_m}{D_{eq}} = \left[0.3 F_{d90} + \left(-0.53 \frac{h_0}{D_{eq}} + 3\right) \right] \cdot \left[\left(-0.01 \left(\frac{h_0}{D_{eq}}\right)^2 + 0.006 \frac{h_0}{D_{eq}} - 0.06\right) \frac{s}{D_{eq}} + 1 \right]$	75°	Pagliara et al. (2011) (3b)
$\frac{z_m}{D_{eq}} = \left[0.3 F_{d90} + \left(-0.46 \frac{h_0}{D_{eq}} + 1.28\right) \right] \cdot \left[\left(-0.03 \frac{h_0}{D_{eq}} - 0.02\right) \frac{s}{D_{eq}} + 1 \right]$	120°	Pagliara et al. (2011) (3c)

$$MAE = \frac{1}{n} \sum_{i=1}^n |O_i - P_i| \tag{21}$$

where P_i is the predicted i th parameter, O_i is the observed i th parameter, and \bar{O} is the mean of observed values.

Results and discussion

At the first stage, a sensitivity analysis was performed to assess the most influential parameters and define the best input combination for the models. For this aim, the most commonly used and the most straightforward network, namely the FFBP, was utilized. The input parameters were fed into the network in dimensional and dimensionless scenarios. At the second stage, the most accurate dimensionless FFBP model identified in the sensitivity analysis with the best input combination was selected and compared with the other corresponding computing approaches (CFBP, RBF, GRNN, ANFIS, and SVR), and the empirical equations from this research and the previous study.

Sensitivity analysis

In this section, the sensitivity analysis results are presented and discussed in the dimensionless and dimensional cases, respectively. The input data were employed in the FFBP model in five steps, and the outputs were evaluated in terms of the CC, NSE, RMSE, and MAE statistics. The bar graphs are also used to facilitate the evaluation.

Non-dimensional case

As can be seen from Table 3 and Fig. 5, the impact of the non-dimensional input variables is assessed by employing them in various combinations.

In step 1, utilizing two parameters of F_{d90} and h_0/D_{eq} led to a model with low accuracy. As can be seen from Table 3, for the scour hole depth prediction, the CC and NSE values are lower than 0.5 for both the training and testing sets (training: CC=0.4684, NSE=0.2154; and testing: CC=0.3735, NSE=0.1191), and the errors (RMSE, MAE) are higher than the other steps. For the location of the maximum scour depth (l_m/D_{eq}), a similar result can be seen.

As S/D_{eq} is added to the model input in the next step, a slight improvement can be seen in the FFBP. For example, for the scour depth (y_m/D_{eq}), the CC increases from 0.4684 to 0.5121 (4.4%) in the training phase and 2.7% in the testing phase; the NSE increases from 0.2154 to 0.2448 in the training phase and grows from 0.1191 to 0.1419 in the testing phase. Also, the RMSE and MAE decrease in step 2. For

Table 3 Quantitative analysis of the dimensionless input combinations on the FFBP

Model (FFBP)	Input combination (non-dimensional)	Scour parameter	Training				Testing			
			CC	NSE	RMSE	MAE	CC	NSE	RMSE	MAE
1	$F_{d90^\circ} \frac{h_0}{D_{eq}}$	y_m/D_{eq}	0.4684	0.2154	0.7118	0.5775	0.3735	0.1191	0.7879	0.6906
		l_m/D_{eq}	0.6022	0.3598	1.2831	0.9846	0.3708	0.0226	1.2998	0.9501
2	$F_{d90^\circ} \frac{h_0}{D_{eq}}, \frac{S}{D_{eq}}$	y_m/D_{eq}	0.5121	0.2448	0.6984	0.5583	0.4007	0.1419	0.7777	0.6886
		l_m/D_{eq}	0.6177	0.3810	1.2617	0.9689	0.3743	0.0041	1.3120	0.9473
3	$F_{d90^\circ} \frac{h_0}{D_{eq}}, \alpha_c$	y_m/D_{eq}	0.7953	0.6318	0.4877	0.4101	0.7812	0.5881	0.5388	0.4580
		l_m/D_{eq}	0.8141	0.6622	0.9321	0.6962	0.7937	0.6197	0.8108	0.6589
4	$F_{d90^\circ} \frac{h_0}{D_{eq}}, \alpha_c, \frac{S}{D_{eq}}$	y_m/D_{eq}	0.9299	0.8609	0.2997	0.2181	0.8714	0.7409	0.4273	0.3170
		l_m/D_{eq}	0.8711	0.7588	0.7877	0.5752	0.8603	0.7321	0.6804	0.5679
5	$F_{d90^\circ} \frac{h_0}{D_{eq}}, \alpha_c, \frac{S}{D_{eq}}, \frac{d90}{D_{eq}}$	y_m/D_{eq}	0.9706	0.9413	0.1948	0.1472	0.9790	0.9556	0.1769	0.1385
		l_m/D_{eq}	0.9401	0.8831	0.5482	0.4170	0.9400	0.8278	0.5456	0.4884

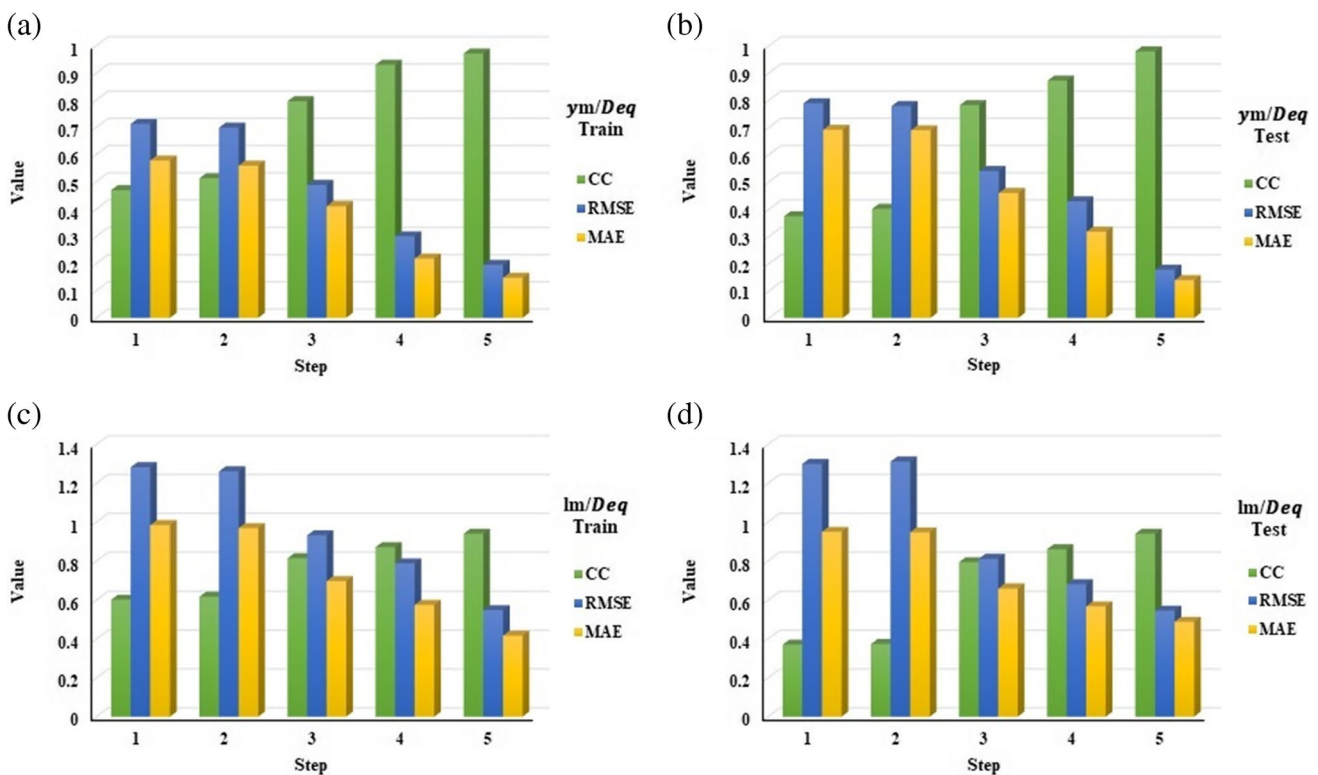


Fig. 5 a–d Sensitivity analysis of the dimensionless parameters on the FFBP

the y_m/D_{eq} , the MAE reduces from 0.6906 to 0.6886 in the testing phase.

In step 3, by eliminating the distance of the crossing point from tailwater level (S/D_{eq}) from the input combination and adding the crossing angle (α_c) instead, a considerable improvement can be seen in the results.

Namely, the prediction of the scour hole depth (y_m/D_{eq}) has a growth of 28% and 38% for the CC in the training and testing datasets. The NSE increases, reaching 0.6318 and 0.5881 in the training and testing sets. The RMSE decreases to 0.4877 and 0.5388 in the training and testing phases, respectively. Furthermore, in step 3, the

Table 4 Quantitative analysis of the dimensional input combinations on the FFBP

Model (FFBP)	Input combination (dimensional)	Scour parameter	Training				Testing			
			CC	NSE	RMSE	MAE	CC	NSE	RMSE	MAE
1	Q, h_0	y_m (m)	0.5310	0.2822	0.0212	0.0173	0.4778	0.2249	0.0230	0.0201
		l_m (m)	0.6311	0.3951	0.0388	0.0296	0.4961	0.1506	0.0377	0.0293
2	Q, h_0, S	y_m (m)	0.5580	0.2976	0.0209	0.0167	0.4809	0.2066	0.0233	0.0208
		l_m (m)	0.6363	0.3943	0.0388	0.0305	0.5336	0.2317	0.0358	0.0295
3	Q, h_0, α_c	y_m (m)	0.8446	0.7096	0.0135	0.0121	0.8609	0.7131	0.0140	0.0125
		l_m (m)	0.8388	0.7032	0.0272	0.0215	0.9044	0.8078	0.0179	0.0142
4	Q, h_0, α_c, S	y_m (m)	0.9719	0.9416	0.0060	0.0048	0.9632	0.9209	0.0073	0.0057
		l_m (m)	0.9006	0.8107	0.0217	0.0160	0.9646	0.8990	0.0130	0.0097
5	$Q, h_0, \alpha_c, S, d_{90}$	y_m (m)	0.9729	0.9447	0.0059	0.0047	0.9625	0.9120	0.0077	0.0063
		l_m (m)	0.9055	0.8156	0.0214	0.0142	0.9681	0.9130	0.0121	0.0102

prediction power for the location of the maximum scour depth (l_m/D_{eq}) improves to about 20% and 42% for the CC, and the NSE value reaches 0.6622 and 0.6197 in the training and testing phases, respectively. Also, a reduction is observed in the errors; the MAE reduces from 0.9689 to 0.6962 in the training phase and from 0.9473 to 0.6589 in the testing phase, respectively.

In step 4, the parameter S/D_{eq} is added again to the combination alongside the α_c , causing the FFBP to obtain better

accuracy, which increases the CC above 86%, about 13% and 10% improvement for y_m/D_{eq} in the training and testing phases, respectively. Estimating the parameter l_m/D_{eq} is also with about 6% and 7% improvement for the CC in the training and testing phases, respectively. The NSE for y_m/D_{eq} and l_m/D_{eq} approaches 0.8609 and 0.7588 in the training set and 0.7409 and 0.7321 in the testing set, respectively.

In step 5, entering the sediment diameter as d_{90}/D_{eq} ended up with the most accurate dimensionless scenario.

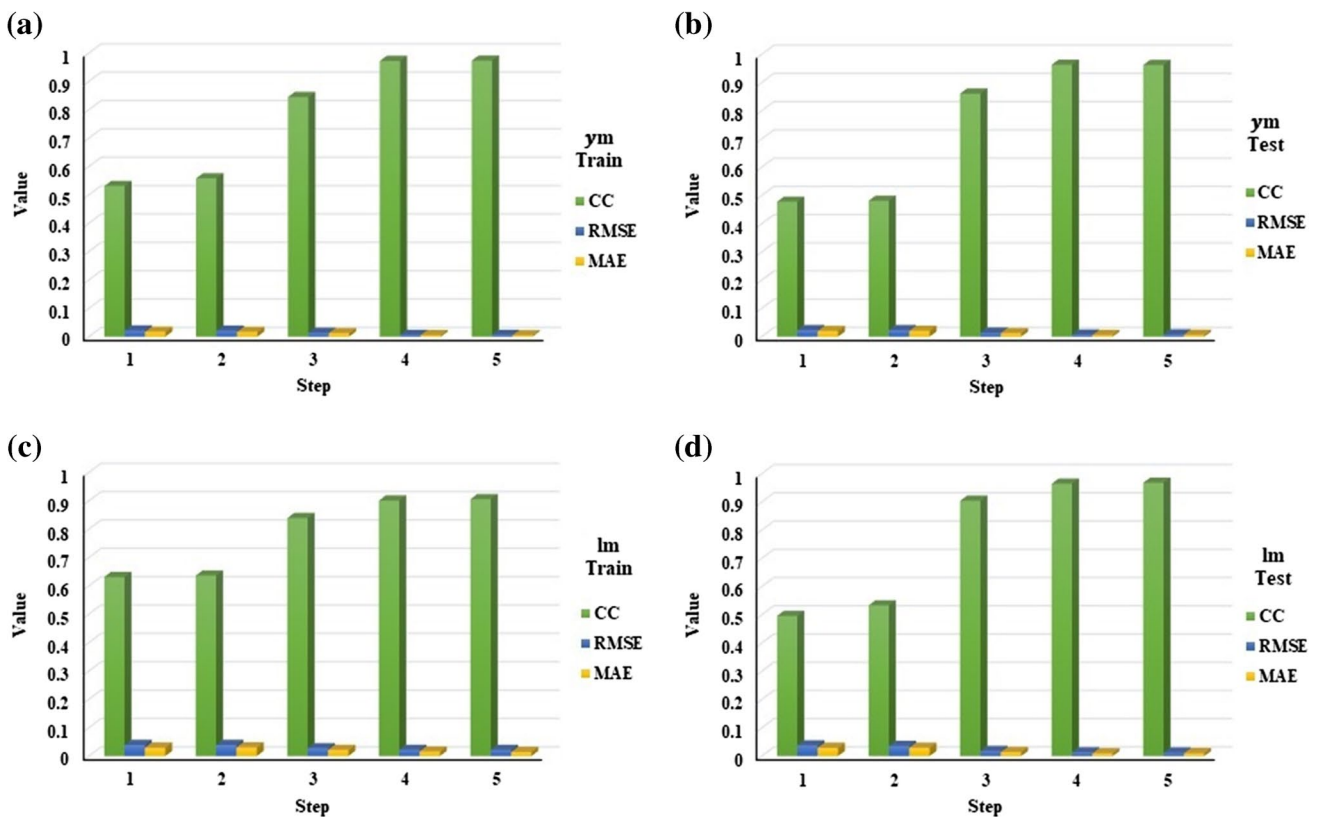


Fig. 6 a–d Sensitivity analysis of the dimensional parameters on the FFBP

Table 5 Parameters of the machine learning models

Parameters					
Model	Architecture			transfer function	
FFBP	5-6-2			Tansig-linear	
CFBP	5-5-2			Tansig-linear	
RBF	5-59-2			Spread=0.055	
GRNN	5-87-2			Spread=0.55	
ANFIS	y_m/D_{eq}			l_m/D_{eq}	
	NO. of mem functions	Range of influence	NO. of mem functions	Range of influence	
	87	0.5	87	0.5	
SVR	y_m/D_{eq}			l_m/D_{eq}	
	γ	σ	γ	r	deg
	107513.48	25.36	0.0411	0.9694	3

In the case of the scour hole depth, the CC increases to 0.9706 and 0.9790 for the training and testing phases, respectively, i.e., about 4% and 10.8%. The NSE reaches its maximum value (NSE=0.9413 and 0.9556). The value of the RMSE and MAE also decreased for both the training and testing states compared to step 4.

Dimensional case

In the case of the dimensional scenario, the trends are almost similar to the dimensionless case. From Table 4 and Fig. 6, this can be observed that by adding the input parameters one by one, the output error decreases, and better accuracy is achieved.

In step 1, using two parameters of Q and h_0 yielded the weakest model, but compared with the corresponding step 1 in the dimensionless form, it has given better results. For instance, considering the testing dataset, the prediction power has improved over its dimensionless one by about 10% and 12% in the CC for the y_m and l_m , respectively; the NSE also has higher values (0.2822 and 0.2249). In step 2, the S parameter has had a marginal impact similar to its dimensionless form and has not changed the accuracy considerably. By eliminating the S and entering the crossing angle (α_c) in the combination (step 3), a sudden increase in the model accuracy is apparent. Accordingly, the CC for y_m improves to 29% and 38% in the training and testing phases, and for l_m increases to 20% and 37% in the training and testing phases, respectively. The NSE value reaches above 0.7 (e.g., in the testing phase, NSE=0.7131 and 0.8078). The errors (RMSE, MAE) also show lower values in the training and testing sets. In step 4, the S parameter has a good influence on the prediction results; the precision level for the CC in all the models reaches above 90%; for the testing set, it is above 96% in both the y_m and l_m . The NSE reaches above 0.9 and 0.8 for the y_m and l_m , respectively. This combination has

higher precision than its corresponding dimensionless case, in the testing phase for y_m (RMSE=0.0073, MAE=0.0057) and for l_m (RMSE=0.0130, MAE=0.0097). As can be seen, the effect of sediment diameter d_{90} on the model in step 5 is marginal, and makes no difference in the results; the CC and NSE values are very close to those in step 4.

From the analysis of the various non-dimensional and dimensional parameters, it is revealed that the crossing angle (α_c) has the highest impact on the predictions as far as the scour maximum depth and its location are concerned. However, for accurate and reliable estimation, it would be better to use all the independent variables.

Comparison of different soft computing methods

The sensitivity analysis results showed that the FFBP model in step 5 with a five-input combination is the most accurate scheme in the non-dimensional impact analysis. Therefore, this dimensionless model is illustrated as FFBP* and would be compared with the other corresponding soft computing schemes (CFBP, RBF, GRNN, ANFIS, and SVR) having the same input combination. The results are also compared with the corresponding regression equations ((16), (17) and Pagliara et al. (2011)’s formulae). The properties of each computational model can be seen in Table 5. Table 6 shows the results in terms of the statistical measures.

Comparing the results for predicting the scour hole depth, the superiority of the SVR can be seen in the testing phase. The SVR estimates the scour hole depth (y_m/D_{eq}) with higher CC =0.9848 and NSE=0.9659 and lower errors (RMSE=0.1549, MAE=0.1167), compared with the other methods, including the regression ones; it also shows a good performance in the training phase with the CC=0.998, NSE=0.9960, and RMSE=0.0505. In the case of the maximum scour hole location (l_m/D_{eq}), the SVR also works better than the other schemes in the testing dataset with higher NSE (0.8348) and lower errors (RMSE=0.5344,

Table 6 The performance results for different soft computing schemes and regression models

Model (FFBP)	Input combination	Scour parameter	Training				Testing			
			CC	NSE	RMSE	MAE	CC	NSE	RMSE	MAE
FFBP*	$(F_{d90}, \frac{h_0}{D_{eq}}, \alpha c, \frac{S}{D_{eq}}, \frac{d90}{D_{eq}})$	y_m/D_{eq}	0.9706	0.9413	0.1948	0.1472	0.9790	0.9556	0.1769	0.1385
		l_m/D_{eq}	0.9401	0.8831	0.5482	0.4170	0.9400	0.8278	0.5456	0.4884
CFBP		y_m/D_{eq}	0.9522	0.9052	0.2475	0.2000	0.9651	0.9302	0.2218	0.1886
		l_m/D_{eq}	0.9132	0.8283	0.6645	0.4733	0.9336	0.7729	0.6266	0.5380
RBF		y_m/D_{eq}	0.9832	0.9667	0.1467	0.1053	0.8305	0.6400	0.5037	0.4224
		l_m/D_{eq}	0.9841	0.9684	0.2850	0.2145	0.7062	0.2116	1.1674	0.9476
GRNN		y_m/D_{eq}	0.9572	0.8716	0.2879	0.2331	0.6617	0.4310	0.6333	0.5299
		l_m/D_{eq}	0.9439	0.8529	0.6150	0.4755	0.6036	0.3038	1.0970	0.8418
ANFIS		y_m/D_{eq}	0.9999	0.9999	1.31e-07	8.06e-08	0.9779	0.9481	0.1912	0.1587
		l_m/D_{eq}	0.9999	0.9999	2.83e-07	1.92e-07	0.9315	0.8075	0.5769	0.4633
SVR		y_m/D_{eq}	0.9980	0.9960	0.0505	0.0377	0.9848	0.9659	0.1549	0.1167
		l_m/D_{eq}	0.9050	0.8176	0.6849	0.4990	0.9231	0.8348	0.5344	0.4201
Regression model Eqs. (16), (17)		y_m/D_{eq}	0.6482	0.4188	0.6121	0.4929	0.5129	0.2540	0.7252	0.6270
		l_m/D_{eq}	0.6940	0.4818	1.1540	0.8751	0.6060	0.3273	1.0779	0.8628
Pagliara et al. (2011) Eq. [(3a)+ (3b)+ (3c)]	$(F_{d90}, \frac{h_0}{D_{eq}}, \frac{S}{D_{eq}})$	y_m/D_{eq}	0.7615	-0.5787	1.0097	0.7819	0.6939	-0.8440	1.1400	0.8796
		l_m/D_{eq}	-	-	-	-	-	-	-	-

MAE=0.4201), but it works weakly in the training phase (CC=0.9050 and RMSE=0.6849).

The FFBP* also estimates the scour hole depth (y_m/D_{eq}) with high accuracy with the CC =0.9790, NSE=0.9556, and RMSE=0.1769 in the testing phase. In the training phase, y_m/D_{eq} prediction is with the NSE=0.9413 and RMSE =0.1948. Also, this is the case for the l_m/D_{eq} parameter in the testing phase; for instance, the estimation power for this parameter in the FFBP* is satisfactory compared with the other schemes (CC=0.94, NSE=0.8278, and RMSE=0.5456).

In the case of the ANFIS, it emerges very powerful in the training phase with the CC=0.9999, NSE=0.9999, and lowest RMSE and MAE values for both y_m/D_{eq} and l_m/D_{eq} features. It also performs well in the testing dataset with CC=0.9779, NSE=0.9481, and MAE=0.1587 for y_m/D_{eq} and CC=0.9315, NSE=0.8075, and MAE=0.4633 for l_m/D_{eq} , respectively.

Alternatively, in the case of the CFBP network, it shows proper scour estimation in both the calibrating and testing phases (CC>0.9); however, it performed relatively poorly in the testing phase compared with the models mentioned above (SVR, FFBP*, and ANFIS). But it yielded better results than the RBF and GRNN with the CC= 0.9651, NSE=0.9302, and MAE=0.1886 for y_m/D_{eq} , and CC=0.9336, MAE=0.5380 for l_m/D_{eq} , respectively, in the testing dataset. In the training phase, it predicts the maximum scour depth and its location with lower NSE (0.9052 and 0.8283) and higher errors than the RBF scheme.

Considering the RBF scheme, it fails to estimate the scour features precisely and performs poorly in the testing phase (CC<0.84, NSE<0.65). It can be seen that the RBF predicts y_m/D_{eq} in the training phase more accurately (CC=0.9832, NSE=0.9667, and MAE=0.1053) than in its testing phase (CC = 0.8305, NSE=0.64, and MAE=0.4224), showing a difference of about 15% in terms of the CC. Also, this is the case for l_m/D_{eq} ; it has about 18% better performance in the training dataset with the CC.

The GRNN also shows this drawback in the testing phase (CC<0.67, NSE<0.44); for example, in the case of y_m/D_{eq} , it has adapted itself well to the training dataset with the NSE=0.8716 and MAE=0.2331; but has acted weak in the testing phase with the NSE=0.4310 and MAE=0.5299. And shows a drop to about 29% for the CC. For l_m/D_{eq} prediction, the difference between the training and testing phases is about 34% with the CC. The GRNN and regression model precision levels for the l_m/D_{eq} parameter in the testing phase are approximately the same.

It can be said that the RBF and GRNN models represent a weak generalization as they cannot estimate the unknown scour hole samples in the testing dataset at a satisfactory level.

The regression models demonstrate a poor performance compared to the machine learning methods, especially the FFBP*, SVM, and ANFIS schemes. The CC for y_m/D_{eq} and l_m/D_{eq} in the calibrating (training) phase is 0.6482 and 0.694, respectively, with NSE<0.5, with higher errors than the AI

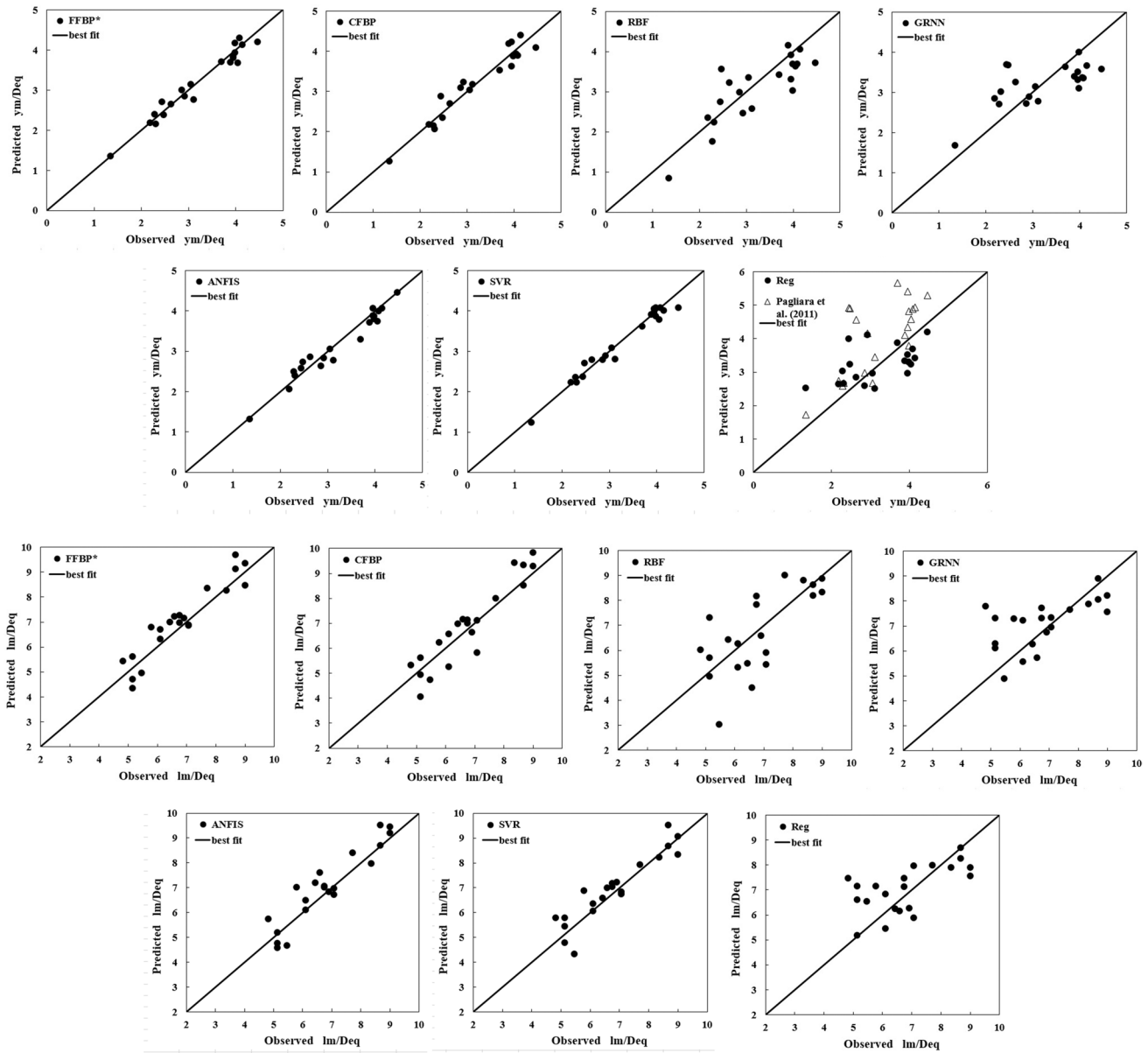


Fig. 7 Scatter plots of experimental versus computed values of y_m/D_{eq} and l_m/D_{eq} with different techniques

models. In the testing phase, the CC for the maximum scour hole depth and its location reaches 0.5129 and 0.606, respectively, with $NSE < 0.33$. These traditional equations show a high difference from the SVR in the CC to about 47% for y_m/D_{eq} and 34% for l_m/D_{eq} . It is concluded that the regression models fail to estimate the scour hole characteristics precisely at the various arbitrary crossing angles. Pagliara et al. (2011) formulae also show poor prediction compared with the developed models of this study, including the regression equation (16). While the CC for the scour hole depth reaches 0.7615 and 0.6939 in the training and testing phases, respectively, the NSE values are negative (-0.5787 and -0.8440), and their errors are high (e.g., $RMSE = 1.0097$ and 1.1400 in the

training and testing phases, respectively). For more evaluation of the performance results of the various applied models, the scatter plots between the experimental and predicted values in the testing dataset are also utilized. The scatter plots of y_m/D_{eq} and l_m/D_{eq} parameters are shown in Fig. 7.

As can be seen from Fig. 7, for y_m/D_{eq} and l_m/D_{eq} , it is revealed that the points are closer to the ideal fit line and less scattered in the FFBP*, ANFIS, and SVR models showing their higher accuracy. As per Fig. 7, these models predict the scour hole depth better than its location. By contrast, in the other approaches (RBF, GRNN, and regression formulae), the points are more scattered than the ideal line, which denotes their lower efficiency in the scour features estimation. It is

Fig. 8 Graph of experimental and computed values of maximum scour depth with machine learning and empirical methods

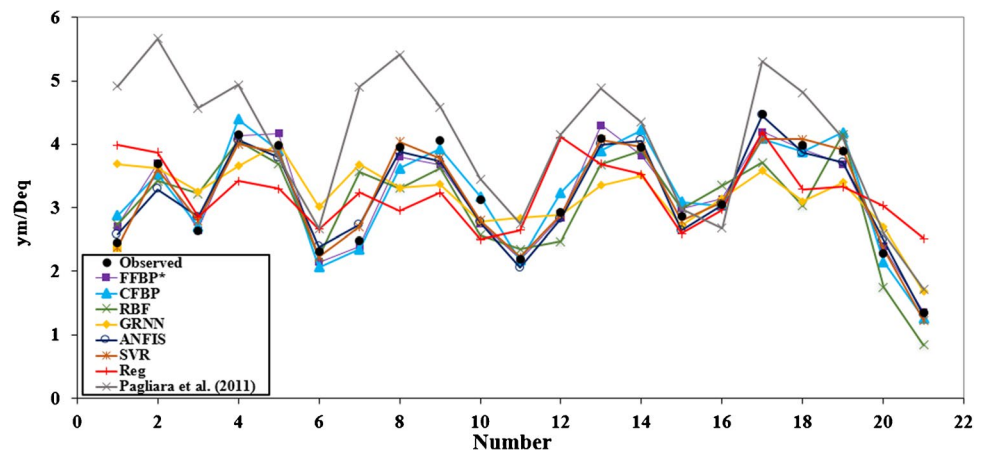
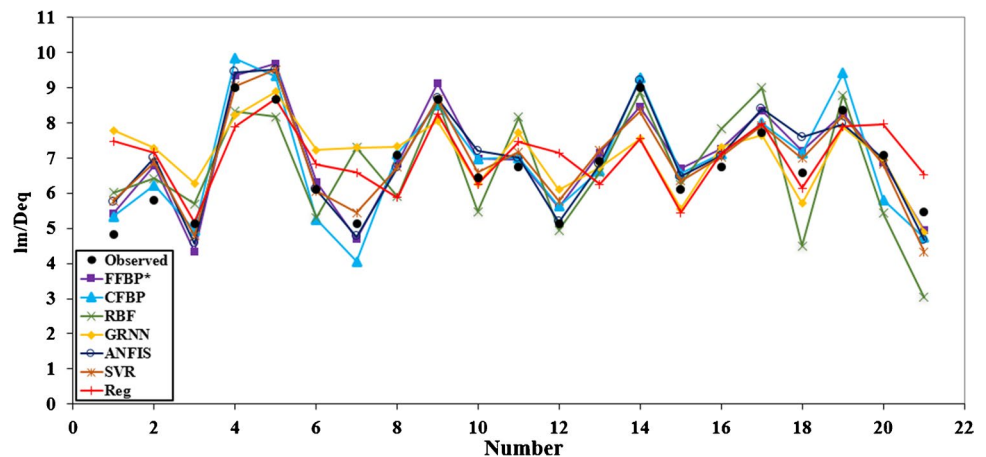


Fig. 9 Graph of experimental and computed values of maximum scour depth location with machine learning and empirical methods



also apparent that Pagliara et al. (2011) equations overestimate the scour hole depth values (y_m/D_{eq}).

The predicting performance of the models in the testing dataset can also be seen in the graphs in Figs. 8 and 9 for y_m/D_{eq} and l_m/D_{eq} , respectively. As can be seen from Fig. 8, the FFBP*, ANFIS, and SVR are superior to the other schemes being closer to the experimental values. However, the SVR has acted slightly better. The deficiency of the GRNN and regression models is evident, estimating the values farther than the experimental data.

The results of this research indicate how the applied AI methods improve further the scour estimations below the crossing jets. One of the advantages of the SVR over the other conventional computing techniques is that it is less time-consuming, less sensitive, and more practical in the engineering fields (Goyal and Ojha 2011).

Conclusions

In the present research, a new approach is presented in the form of the ANNs (FFBP, CFBP, RBF, and GRNN), ANFIS, and SVR to predict the principal characteristics

of the scour hole below the symmetric crossing jets. The maximum scour depth with its location relative to the origin was investigated. Most of the previous studies have been carried out on single jets, with a few dealing with crossing jets. The problem with the regression models is that they fail to predict the scour features precisely due to the complicated phenomenon. Hence, this research addressed this issue using soft computing techniques and compared the results with the conventional regression equations. The results demonstrate that the applied AI methods outperform the regression models.

The sensitivity analysis results on the FFBP network show that in both scenarios, the crossing angle (α_c) is the most influential parameter. In the non-dimensional case, using an input combination containing all of the input parameters (5 inputs) leads to the most accurate model and is needed for a satisfying estimation. On the other hand, in the dimensional case, it is concluded that using four inputs (Q, h_0, α_c, S) suffices for a good prediction.

It is found that considering the crossing angle as an independent parameter in the regression model cannot provide powerful models capable of predicting the scour at multiple arbitrary crossing angles. By contrast,

the SVR, FFBP*, and ANFIS remarkably improved the results and estimated the unknown values of the scour hole depth and its location more accurately. The SVR was superior to the other schemes in the testing phase. By employing the SVR, the difference between its performance with that of the derived regression models reached 47% and 31.71% for y_m/D_{eq} and l_m/D_{eq} parameters, respectively, in terms of the CC. Also, their NSE reached 0.9659 and 0.8348. It is concluded that the developed AI schemes can be successfully employed as robust and efficient alternative methods for predicting the scour below two symmetric crossing jets. This research was conducted in laboratory conditions, and the results may be limited to the experimental scales. However, the developed models may be helpful for the design of plunge pools under similar conditions.

Declarations

Conflict of interest The authors declare no competing interests.

References

- Adib A, Tabatabaee SH, Khademalrasoul A, Mahmoudian Shoushtari M (2020) Recognizing of the best different artificial intelligence method for determination of local scour depth around group piers in equilibrium time. *Arab J Geosci* 13, 1004. [10.1007/s12046-019-1153-6S](https://doi.org/10.1007/s12046-019-1153-6S)
- Azimi H, Bonakdari H, Ebtehaj I, Shabanlou S, Ashraf Talesh SH, Jamali A (2019) A Pareto design of evolutionary hybrid optimization of ANFIS model in prediction abutment scour depth. *J Indian Acad Sci* 44:169. <https://doi.org/10.1007/s12046-019-1153-6S>
- Azmathullah HM, Deo MC, Deolalikar PB (2005) Neural networks for estimation of scour downstream of a ski-jump bucket. *J Hydraul Eng* 13:898–908
- Band SS, Heggy E, Bateni SM, Karami H, Rabiee M, Samadianfard S, Chau KW, Mosavi A (2021) Groundwater level prediction in arid areas using wavelet analysis and Gaussian process regression. *Eng Appl Comput Fluid Mech* 15:1147–1158. <https://doi.org/10.1080/19942060.2021.1944913>
- Bombardelli FA, Palermo M, Pagliara S (2018) Temporal evolution of jet induced scour depth in cohesionless granular beds and the phenomenological theory of turbulence. *Phys Fluids* 30:085109. <https://doi.org/10.1063/1.5041800>
- Bonakdari H, Moradi F, Ebtehaj I, Gharabaghi B, Sattar AA, Azimi AH, Radecki-Pawlik A (2020) A non-tuned machine learning technique for abutment scour depth in clear water condition. *Water (Switzerland)* 12:301. <https://doi.org/10.3390/w12010301>
- Campos JA, Pedrollo OC (2021) A regional ANN-based model to estimate suspended sediment concentrations in ungauged heterogeneous basins. *Hydrol Sci J* 66:1222–1232
- Chen J, Zhang G, Si JH, Shi H, Wang X (2022) Experimental investigation of scour of sand beds by submerged circular vertical turbulent jets. *Ocean Eng* 257:111625. <https://doi.org/10.1016/j.oceaneng.111625>
- Das UK, Roy P, Ghose DK (2019) Modeling water table depth using adaptive neuro-fuzzy inference system. *ISH J Hydraul Eng* 25:291–297
- Ebtehaj I, Bonakdari H, Moradi F, Gharabaghi B, Khozani ZS, Sheikh Khozani Z (2018) An integrated framework of extreme learning machines for predicting scour at pile groups in clear water condition. *Coast Eng* 135:1–15. <https://doi.org/10.1016/j.coastaleng.12.012>
- Goyal MK, Ojha CS (2011) Estimation of scour downstream of a ski-jump bucket using support vector and m5 model tree. *Water Resour Manag J* 25:2177–2195. <https://doi.org/10.1007/s11269-011-9801-6>
- Hassanvand MR, Karami H, Mousavi SF (2018) Investigation of neural network and fuzzy inference neural network and their optimization using meta-algorithms in river flood routing. *Nat Hazards* 94:1057–1080. <https://doi.org/10.1007/s11069-018-3456-z>
- Hassanzadeh Y, Jafari-Bavil-Olyaei A, Aalami MT, Kardan N (2019) Meta-heuristic optimization algorithms for predicting the scouring depth around bridge piers. *Periodica Polytechnica Civil Engineering* 63(3):856–871. <https://doi.org/10.3311/PPci.12777>
- Haykin S (1994) *Neural networks: a comprehensive foundation*. Macmillan
- Hoang ND, Liao KW, Tran XL (2018) Estimation of scour depth at bridges with complex pier foundations using support vector regression integrated with feature selection. *J Civ Struct Heal Monit* 8:431–442
- Hu Z, Karami H, Rezaei A, DadrasAjirlou Y, Piran MJ, Shamshirband S, Chau KW, Mosavi A (2021) Using soft computing and machine learning algorithms to predict the discharge coefficient of curved labyrinth overflows. *Eng Appl Comput Fluid Mech* 15:1002–1015. <https://doi.org/10.1080/19942060.2021.1934546>
- Jang JSR (1993) ANFIS: adaptive-network-based fuzzy inference system. *IEEE Trans Syst Man Cybern J* 23:665–685
- Jang JSR, Sun CT, Mizutani E (1997) *Neuro-fuzzy and soft computing: a computational approach to learning and machine intelligence*. Prentice Hall
- Kartal V, Emiroglu ME (2022) Experimental study of scour morphology from plunging water jets. *Water Supply* 22:5410–5433
- Kaveh K, Mai DN, Pham QB, Tran Anh D (2021) A hybrid feed-forward neural network with grasshopper optimization for observing pattern of scour depth around bridge piers. *Arab J Geosci* 14:2352. <https://doi.org/10.1007/s12517-021-08617-8>
- Latifi A, Hosseini SA, Saneie M (2018) Comparison of downstream scour of single and combined free-fall jets in co-axial and non-axial modes. *J Model Earth Syst Environ* 4:1271–1284
- MacKay DJC (1992) Bayesian interpolation. *Neural Comput* 4:415–447
- Malik A, Kumar A, Kim S, Kashani MH, Karimi V, Sharafati A, Ghorbani MA, Al-Ansari N, Salih SQ, Yaseen ZM (2020) Modeling monthly pan evaporation process over the Indian central Himalayas: application of multiple learning artificial intelligence model. *Eng Appl Comput Fluid Mech* 14:323–338
- McCulloch WS, Pitts W (1943) A logical calculus of the ideas immanent in nervous activity. *Bull Math Biophys* 5:115–133
- Mehraein M, Ghodsian M, Schleiss A (2012) Scour formation due to simultaneous circular impinging jet and wall jet. *J Hydraul Res* 50:395–399
- Mohammadpour R (2017) Prediction of local scour around complex piers using GEP and M5-Tree. *Arab J Geosci* 10(18):416. <https://doi.org/10.1007/s12517-017-3203-x>
- Naini S (2011) Evaluation of RBF, GR and FFBP neural networks for prediction of geometrical dimensions of scour hole below ski-jump spillway. *Intl Conf Environ Comput Sci Singapore* 19:89–93
- Naini S, Karami H, Hoseini K (2022) Experimental investigation and determination of scour dimensions due to symmetric crossing jets. *J Hydraul*. <https://doi.org/10.30482/jhyd.2022.309123.1559>
- Nivesh S, Negi D, Kashyap PS, Aggarwal S, Singh B, Saran B, Sawant PN, Sihag P (2022) Prediction of river discharge of Kesinga sub-catchment of Mahanadi basin using machine learning approaches. *Arab J Geosci* 15:1369. <https://doi.org/10.1007/s12517-022-10555-y>

- Uyumaz A (1988) Scour downstream of the vertical gate. *J Hydraul Eng* 114:811–816
- Parsaie A, Haghiabi AH, Moradinejad A (2019) Prediction of scour depth below river pipeline using support vector machine. *KSCE J Civ Eng* 23:2503–2513
- Pagliara S, Amidei M, Hager WH (2008) Hydraulics of 3D plunge pool scour. *J Hydraul Eng* 134:1275–1284
- Pagliara S, Palermo M (2013) Analysis of scour characteristics in presence of aerated crossing jets. *Aust J Water Resour* 16:163–172
- Pagliara S, Palermo M (2017) Scour process caused by multiple sub-vertical non-crossing jets. *J Water Sci Eng* 10:17–24
- Pagliara S, Roy D, Palermo M (2011) Scour due to crossing jets at fixed vertical angle. *J Irrig Drain Eng* 137:49–55
- Palermo M, Bombardelli FA, Pagliara S, Kuroiwa J (2021) Time-dependent scour processes on granular beds at large scale. *Environ Fluid Mech* 21:791–816. <https://doi.org/10.1007/s10652-021-09798-2>
- Rajaratnam N, Mazurek KA (2002) Erosion of a polystyrene bed by obliquely impinging circular turbulent air jets. *J Hydraul Res* 40:709–716
- Rashki Ghaleh Nou M, Azhdary Moghaddam M, Shafai Bajestan M, Azamathulla HM (2019) Estimation of scour depth around submerged weirs using self-adaptive extreme learning machine. *J Hydroinf* 21:1082–1101. <https://doi.org/10.2166/hydro.2019.070>
- Riahi-Madvar H, Dehghani M, Seifi A, Salwana E, Shamshirband S, Mosavi A, Chau KW (2019) Comparative analysis of soft computing techniques RBF, MLP, and ANFIS with MLR and MNL for predicting grade-control scour hole geometry. *Eng Appl Comput Fluid Mech* 13:529–550. <https://doi.org/10.1080/19942060.2019.1618396>
- Salih SQ, Sharafati A, Khosravi K, Faris H, Kisi O, Tao H, Ali M, Yaseen ZM (2019) River suspended sediment load prediction based on river discharge information: application of newly developed data mining models. *Hydrol Sci J* 65:624–637. <https://doi.org/10.1080/02626667.2019.1703186>
- Sá Machado L, Lima MMCL, Aleixo R, Carvalho E (2019) Effect of the ski jump bucket angle on the scour hole downstream of a converging stepped spillway. *Int J River Basin Manag.* <https://doi.org/10.1080/15715124.2019.1586717>
- Samet K, Hoseini K, Karami H, Mohammadi M (2019) Comparison between soft computing methods for prediction of sediment load in rivers: Maku Dam Case Study. *Iran J Sci Technol Trans Civ Eng* 43:93–103. <https://doi.org/10.1007/s40996-018-0121-4>
- Sammen SS, Ghorbani MA, Malik A, Tikhamarine Y, AmirRahmani M, Al-Ansari N, Chau K-W (2020) Enhanced artificial neural network with Harris Hawks optimization for predicting scour depth downstream of ski-jump spillway. *Appl Sci* 10:516
- Seyedian SM, Riahi-Madvar H, Fatabadi A, Farasati M, Ghaznavi S (2022) Comparative uncertainty analysis of soft computing models predicting scour depth downstream of grade-control structures. *Arab J Geosci* 15:418. <https://doi.org/10.1007/s12517-022-09704-0>
- Shahbazbeygi E, Yosefvand F, Yaghoubi B, Shabanlou S, Rajabi A (2021) Generalized structure of group method of data handling to prognosticate scour around various cross-vane structures. *Arab J Geosci* 14:1121. <https://doi.org/10.1007/s12517-021-07483-8>
- Sharafati A, Haghbin M, Haji Seyed Asadollah SB, Tiwari NK, Al-Ansari N, Yaseen ZM (2020a) Scouring depth assessment downstream of weirs using hybrid intelligence models. *Applied Sciences*, (Basel, Switzerland), 10:3714
- Sharafati A, Haghbin M, Torabi M (2021) Assessment of novel nature-inspired fuzzy models for predicting long contraction scouring and related uncertainties. *Front Struct Civ Eng* 15:665–681
- Sharafati A, Tafarjnoruz A, Yaseen ZM (2020b) New stochastic modeling strategy on the prediction enhancement of pier scour depth in cohesive bed materials. *J Hydroinf* 22(3):457–472. <https://doi.org/10.2166/hydro.2020.047>
- Smola AJ, Scholkopf B (2004) A tutorial on support vector regression. *Stat Comput* 14:199–222
- Specht DF (1991) A general regression neural network. *IEEE Trans Neural Netw* 2:568–576
- Sun X, Bi Y, Karami H, Naini S, Band SS, Mosavi A (2021) Hybrid model of support vector regression and fruitfly optimization algorithm for predicting ski-jump spillway scour geometry. *Eng Appl Comput Fluid Mech* 15:272–291. <https://doi.org/10.1080/19942060.2020.1869102>
- Tao H, Al-Khafaji ZSQ, Zounemat-Kermani M, Kisi O, Tiyasha T et al (2021) Artificial intelligence models for suspended river sediment prediction: state-of-the art, modeling framework appraisal, and proposed future research directions. *Eng Appl Comput Fluid Mech* 15:1585–1612. <https://doi.org/10.1080/19942060.2021.1984992>
- Vapnik V (1995) *The nature of statistical learning theory*. 2nd. Springer
- Yaseen ZM, Allawi MF, Karami H, Ehteram M, Farzin S, Ahmed AN, Koting SB, Mohd NS, Jaafar WZB, Afan HA, El-Shafie A (2019) A hybrid bat–swarm algorithm for optimizing dam and reservoir operation. *Neural Comput & Applic* 31:8807–8821. <https://doi.org/10.1007/s00521-018-3952-9>
- Yaseen ZM (2020) Integrative stochastic model standardization with genetic algorithm for rainfall pattern forecasting in tropical and semi-arid environments. *Hydrol Sci J* 65:1145–1157

Springer Nature or its licensor (e.g. a society or other partner) holds exclusive rights to this article under a publishing agreement with the author(s) or other rightsholder(s); author self-archiving of the accepted manuscript version of this article is solely governed by the terms of such publishing agreement and applicable law.